

New MIKE Observations of $z < 1.5$ Sub-Damped Lyman- α Systems

Joseph D. Meiring^{1*}, Varsha P. Kulkarni¹, James T. Lauroesch², Celine Péroux³, Pushpa Khare⁴, & Donald G. York^{5,6}

¹*Department of Physics and Astronomy, University of South Carolina, Columbia, SC 29208, USA*

²*Department of Physics and Astronomy, University of Louisville, Louisville, Ky 40292 USA*

³*Laboratoire d'Astrophysique de Marseille, OAMP, Université Aix-Marseille & CNRS, 13388 Marseille cedex 13, France*

⁴*Department of Physics, Utkal University, Bhubaneswar, 751004, India*

⁵*Department of Astronomy and Astrophysics, University of Chicago, Chicago, IL 60637, USA*

⁶*Enrico Fermi Institute, University of Chicago, Chicago, IL 60637, USA*

Accepted ... Received ...; in original form ...

ABSTRACT

The Damped and sub-Damped Lyman- α (DLA and sub-DLA) systems seen in the spectra of QSOs offer a unique way to study the interstellar medium of high redshift galaxies. In this paper we report on new abundance determinations in a sample of 10 new systems, nine of the lesser studied sub-DLAs and one DLA, along the line of sight to seven QSOs from spectra taken with the MIKE spectrograph. Lines of Mg I, Mg II, Al II, Al III, Ca II, Mn II, Fe II, and Zn II were detected. Here, we give the column densities and equivalent widths of the observed absorption lines, as well as the abundances determined for these systems. Zn, a relatively undepleted element in the local interstellar medium (ISM) is detected in one system with a high metallicity of $[\text{Zn}/\text{H}] = +0.27 \pm 0.18$. In one other system, a high abundance based on the more depleted element Fe is seen with $[\text{Fe}/\text{H}] = -0.37 \pm 0.13$, although Zn is not detected. The $N_{\text{H I}}$ -weighted mean metallicity of these sub-DLA systems based on Fe is $\langle [\text{Fe}/\text{H}] \rangle = -0.76 \pm 0.11$, nearly ~ 0.7 dex higher (a factor of 5) than what is seen in DLAs in this redshift range. The relative abundance of $[\text{Mn}/\text{Fe}]$ is also investigated. A clear trend is visible for these systems as well as systems from the literature, with $[\text{Mn}/\text{Fe}]$ increasing with increasing metallicity in good agreement with Milky Way stellar abundances.

Key words: Quasars: absorption lines-ISM: abundances

1 INTRODUCTION

Quasar absorption line systems with strong Lyman- α lines are often divided into two classes: Damped Lyman- α (DLAs, $\log N_{\text{H I}} \geq 20.3$) and sub-Damped Lyman- α (sub-DLA $19 \lesssim \log N_{\text{H I}} < 20.3$, Péroux et al. 2001) which contain a major fraction of the neutral gas in the Universe, while the majority of the baryons are thought to lie in the highly ionized and diffuse Lyman- α forest clouds with $\log N_{\text{H I}} \lesssim 15$ in intergalactic space (Petitjean et al. 1993; Danforth & Shull 2008). The lower threshold of $\log N_{\text{H I}} = 20.3$ for classification of DLAs stems from previous 21 cm emission studies of nearby spirals, where the sensitivity limited column density

of $\log N_{\text{H I}} \sim 20.3$ was seen to lie near the Holmberg radius ($R_{26.5}$) of the galaxy Bosma (1981). Nonetheless, the damping wings which can be used to accurately measure $N_{\text{H I}}$ in these systems do begin the sub-DLA regime of $\log N_{\text{H I}} \gtrsim 19.0$. With their high gas content, the DLA and sub-DLA systems are believed to be associated directly with galaxies at all redshifts in which they are seen.

Among the many elements often detected in QSO absorber systems including C, N, O, Mg, Si, S, Ca, Ti, Cr, Mn, Fe, Ni, and Zn, Zn is the preferred tracer of the gas-phase metallicity as it is relatively undepleted in the Galactic ISM, especially when the fraction of H in molecular form is low, as is the case in most DLAs. Zn also tracks the Fe abundance in Galactic stars (e.g., Nissen et al. (2004)), and the lines of Zn II $\lambda\lambda$ 2026, 2062 are relatively weak and typically unsaturated. These lines can be covered with ground

* Current Address: Department of Physics and Astronomy, University of Louisville, Louisville Ky 40292

based spectroscopy over a wide range of redshifts, $0.65 \lesssim z \lesssim 3.5$, which covers a large portion ($\sim 45\%$) of the history of the Universe. Abundances of refractory elements such as Cr and Fe relative to Zn also give a measure of the amount of dust depletion (York et al. 2006). Abundance ratios such as [Si/Fe], [O/Fe] and [Mn/Fe] shed light on the enrichment from the different types of supernovae, as the α -capture elements Si and O for example are produced mainly in Type II explosions while the iron peak elements are produced mainly by Type Ia supernovae.

In previous studies, DLA systems have been the preferred systems for chemical abundance investigation owing to their high gas content (Prochaska & Wolfe 2002; Kulkarni et al. 2005; Meiring et al. 2006). Most DLAs however have been found to be metal poor, typically far below the solar level and below where models predict the mean metallicity should be at the corresponding redshifts at which they are seen (e.g., Kulkarni et al. (2005) and references therein). The sub-DLA systems have until recently been largely ignored, with their contribution to the overall metal budget unknown. Evidence for the possibility of a non-negligible contribution from sub-DLAs to the metal budget came from Péroux et al. (2003a), who noted that based on Fe II lines the sub-DLA systems have faster evolution of the Fe abundance and higher abundances on average than DLA systems. This has also been validated by Kulkarni et al. (2007).

Galactic chemical evolution is a slow process, and long timescales must be examined to search for the signs of the gradual chemical enrichment that models predict (Cen et al. 2003; Pei, Fall, & Hauser 1999). Although redshifts $z < 1.5$ span $\sim 70\%$ of the age of the Universe (using a concordance cosmology of $\Omega_m = 0.3$, $\Omega_\Lambda = 0.7$, $H_0 = 70 \text{ km s}^{-1} \text{ Mpc}^{-1}$), few observations have been made of $z < 1.5$ sub-DLAs due to the lack of spectrographs with enough sensitivity in short wavelengths and the paucity of known sub-DLAs in this redshift range. With such a large fraction of the age of the Universe covered in the redshift regime, it is clearly important for understanding the nature of sub-DLA systems and galactic chemical evolution as well.

We have greatly increased the sample of sub-DLAs in past several years with our VLT UVES and Magellan-II MIKE spectra. In this paper, we report on ten new systems observed with the MIKE spectrograph on the Magellan-II Clay telescope. The structure of this paper is as follows: In § 2, we discuss details of our observations and data reduction techniques. § 4 gives details on the individual objects in these new observations. § 5 investigates the ratio of [Mn/Fe] in QSO absorbers. In § 6 we discuss the abundances of these absorbers and we give a brief discussion. We also provide an appendix at the end of this paper, showing plots of the UV spectra with the fits to the Lyman- α lines, and tables containing the fit parameters for the individual systems.

2 OBSERVATIONS AND DATA REDUCTION

The observations presented here were made with the 6.5m Magellan-II Clay telescope and the Magellan Inamori Kyocera Echelle (MIKE) spectrograph (Bernstein et al. 2003) in 2007 Sep. This is a double sided spectrograph with both a blue and a red camera, providing for simultaneous wave-

length coverage from $\sim 3340 \text{ \AA}$ to $\sim 9400 \text{ \AA}$. Targets were observed in multiple exposures of 1800 to 2700 sec each to minimize cosmic ray defects. The seeing was typically $< 1''$, averaging $\sim 0.7''$. All of the target QSOs were observed with the $1'' \times 5''$ slit and the spectra were binned 2×3 (spatial by spectral) during readout. The resolving power of the MIKE spectrograph is $\sim 19,000$ and $\sim 25,000$ on the red and blue sides respectively with a $1''$ slit. Table 1 gives a summary of the observations.

These spectra were reduced using the MIKE pipeline reduction code in IDL developed by S. Burles, J. X. Prochaska, and R. Bernstein. Wavelengths were calibrated using a Th-Ar comparison lamp taken after each exposure. The data were first bias subtracted from the overscan region and flat-fielded. The data were then sky-subtracted and the spectral orders were extracted using the traces from flat field images. These extracted spectra were then corrected for heliocentric velocities and converted to vacuum wavelengths. Each individual order was then combined in IRAF using rejection parameters to reduce the effects of cosmic rays. These combined spectra were then normalized using a polynomial, typically of order five or less, or spline function to fit the continuum.

Our new observations consists of 10 absorbers, nine sub-DLAs and one DLA $z_{abs} \lesssim 1.5$. See Meiring et al. (2008) for a discussion of our selection criteria. Throughout this paper the QSO names are given in J2000 coordinates, except in Table 1 where the original name, based on J1950 coordinates is also given if applicable (Hewitt & Burbidge 1987).

3 DETERMINATION OF COLUMN DENSITIES

Column densities were determined from profile fitting with the package FITS6P (Welty et al. 1991), which has evolved from the code by Vidal-Madjar et al. (1977). FITS6P iteratively minimizes the χ^2 value between the data and a theoretical Voigt profile that is convolved with the instrumental profile. The profile fit used multiple components, tailored to the individual system. For the central, core components, the effective Doppler parameters (b_{eff}) and radial velocities were determined from the weak and unsaturated lines, typically the Mg I λ 2852 line. For the weaker components at higher radial velocities the b_{eff} and component velocity values were determined from stronger transitions such as the Fe II $\lambda\lambda$ 2344, 2382 lines and the Mg II $\lambda\lambda$ 2796, 2803 lines. A set of b_{eff} and v values were thus determined that reasonably fit all of the lines observed in the system. The same b_{eff} values were used for all the species. The atomic data used in line identification and profile fitting are from Morton (2003).

In general, if a multiplet was observed, the lines were fit simultaneously until convergence. For all of the systems, the Fe II $\lambda\lambda$ 2344, 2374, 2382 lines were fit simultaneously to determine a set of column densities that fit the spectra reasonably well. Similarly, the Mg II $\lambda\lambda$ 2796, 2803 lines were also fit together. Significant saturation of the Mg II $\lambda\lambda$ 2796, 2803 and Al II λ 1670 lines allowed for only lower limits to be placed on the column densities for these species. The Zn II λ 2026.137 line is blended with a line of Mg I λ 2026.477. The Mg I contribution to the line was estimated using the

QSO J2000	Original or SDSS ID	RA	Dec	m_V or m_g	z_{em}	z_{abs}	$N_{H\ I}$ cm^{-2}	Exposure Time Sec
Q0005+0524	Q0002+051	00:05:20.21	+05:24:10.8	16.9 ^a	1.899	0.8514	19.08 ± 0.04	3600
Q0012-0122	Q0009-016	00:12:10.89	-01:22:07.5	18.1 ^a	1.998	1.3862	20.26 ± 0.03	5400
Q0021+0104	SDSS J002127.88+010420.2	00:21:27.88	+01:04:20.1	18.6 ^b	1.829	1.3259	20.04 ± 0.11	8100
...	1.5756	20.48 ± 0.15	...
Q0427-1302	Q0424-131	04:27:07.32	-13:02:53.6	17.5 ^a	2.166	1.4080	19.04 ± 0.04	12300
Q1631+1156	Q1629+120	16:31:45.24	+11:56:02.9	18.6 ^b	1.792	0.9004	19.70 ± 0.04	13500
Q2051+1950	Q2048+196	20:51:45.87	+19:50:06.3	18.5 ^a	2.367	1.1157	20.00 ± 0.15	13500
Q2352-0028	SDSS J235253.51-002850.4	23:52:53.51	-00:28:51.3	18.5 ^b	1.628	0.8730	19.18 ± 0.09	13500
...	1.0318	19.81 ± 0.13	...
...	1.2467	19.60 ± 0.24	...

Table 1: Summary of Observations. ^a m_V , ^b m_g

Mg I λ 2852 line, for which $f\lambda$ is ~ 32 times that of the Mg I λ 2026 line. The Zn II components were then allowed to vary while the Mg I components were held fixed. $N_{Cr\ II}$ was determined by simultaneously fitting the Cr II λ 2056 line and the blended Cr II + Zn II λ 2062 line, where the contribution from Zn II was estimated from the Zn II + Mg I λ 2026 line. See also Khare et al. (2004) and Meiring et al. (2007, 2008) for a discussion of the profile fitting scheme. We adopt the standard notation:

$$[X/H] = \log(N_X/N_{H\ I}) - \log(X/H)_\odot \quad (1)$$

Solar system abundances have been adopted from Lodders (2003). As the Lyman- α lines from which we can determine $N_{H\ I}$ all lie in the UV, even when redshifted, space based UV spectra are necessary. Neutral Hydrogen column densities were determined from archived HST STIS and FOS spectra available from the HST archives. These systems have previously had $N_{H\ I}$ determined in Rao, Turnshek, & Nestor (2006), although the plots for the sub-DLAs are not published. We give in the Appendix the plots of the Lyman- α lines for these systems with the fits overlaid. In general, the fits from Rao, Turnshek, & Nestor (2006) and our determinations agree quite well. However, for Q2051+1960 we have determined a different value of $N_{H\ I} = 20.00 \pm 0.15$. In all other cases, we have used the values from Rao, Turnshek, & Nestor (2006). Rest frame equivalent widths for the lines are given in Table 2, with 3σ upper limits based on the photon noise and continuum level given in cases without a detection.

4 NOTES ON INDIVIDUAL OBJECTS

4.0.1 Q0005+0524 ($z_{em} = 1.899$)

(System A: $z_{abs} = 0.8514$): This fairly bright QSO has a weak sub-DLA system with $\log N_{H\ I} = 19.08$ in the spectrum (Rao, Turnshek, & Nestor 2006). Eight components were needed to fit the observed profiles. Lines of Mg I λ 2852, Mg II $\lambda\lambda$ 2796, 2803, Al III $\lambda\lambda$ 1854, 1862, and Fe II $\lambda\lambda$ 2344, 2374, 2382, 2586, 2600 were detected. No Zn II $\lambda\lambda$ 2026, 2052 lines were detected with $S/N \sim 50$ in the region. An upper limit of $[Zn/H] < -0.47$ was placed based on the noise in the region. Based on Fe, the metallicity for this system is $[Fe/H] = -0.76 \pm 0.04$. With the relatively low value of Fe II/Al III = $+0.68 \pm 0.04$, there could be signifi-

cant ionisation in the system. Velocity plots of several lines are shown in Figure 1.

4.0.2 Q0012-0122 ($z_{em} = 1.998$)

(System A: $z_{abs} = 1.3862$): This system is a sub-DLA with $\log N_{H\ I} = 20.26$ (Rao, Turnshek, & Nestor 2006). Lines of Mg I λ 2852, Mg II $\lambda\lambda$ 2796, 2803, Al II λ 1670, Al III $\lambda\lambda$ 1854, 1862, Si II λ 1526 and Fe II $\lambda\lambda$ 2344, 2374, 2382, 2586, 2600 were all detected. This system shows minimal α enhancement with $[Si/Fe] = +0.12 \pm 0.08$. Detections of both the Al III and Al II lines in this system show that Al III/Al II < -0.19 . This system appears to be fairly metal poor. No Zn II $\lambda\lambda$ 2026, 2062 lines were detected and an upper limit of $[Zn/H] < -1.34$ was determined for this system. Based on Fe, the metallicity is $[Fe/H] = -1.49 \pm 0.02$. Velocity plots of several lines are shown in Figure 2.

4.0.3 Q0021+0104 ($z_{em} = 1.829$)

(System A: $z_{abs} = 1.3259$): This is a sub-DLA system with $\log N_{H\ I} = 20.04$ (Rao, Turnshek, & Nestor 2006). We detect lines of Mg I λ 2852, Mg II $\lambda\lambda$ 2796, 2803, Al II λ 1670, Al III $\lambda\lambda$ 1854, 1862, Si II λ 1526 and Fe II $\lambda\lambda$ 2344, 2374, 2382, 2586, 2600. The Mn II λ 2576 was also possibly detected at a $\sim 2\sigma$ level. The complex absorption profile required profile required 13 components for an adequate fit. The Si II λ 1808 and Al III $\lambda\lambda$ 1854, 1862 lines fell in portions of the detector with serious cosmetic issues, so they could not be measured. No Zn II lines are present in the spectra with $S/N \sim 25$ in the region. The metallicity based on Zn is thus $[Zn/H] < -1.19$. Simultaneous fits to the Fe II lines provide a measure of the Fe metallicity as $[Fe/H] = -0.82 \pm 0.11$. Due to the saturation of the Si II λ 1526 line, only a lower limit could be placed on the column density. Even with this lower column density, the system shows signs of α enhancement with $[Si/Fe] > +0.14$. Velocity plots of several lines are shown in Figure 3.

(System B: $z_{abs} = 1.5756$): This system is a DLA with $\log N_{H\ I} = 20.48$ (Rao, Turnshek, & Nestor 2006). The complex velocity profile spanned $\sim 600 \text{ km s}^{-1}$ in velocity space, and required 20 components in the fitting. Lines of Mg I λ 2852, Mg II $\lambda\lambda$ 2796, 2803, Al III $\lambda\lambda$ 1854, Si II λ 1526 and Fe II $\lambda\lambda$ 1608, 2344, 2374, 2382, 2586, 2600. The Fe II $\lambda\lambda$ 1608, 2374 lines were weak enough that accurate column densities could be determined. This DLA has a metallicity from Fe of

Table 2: Rest frame equivalent widths and 1σ errors of the observed absorption lines in mÅ.

QSO	z_{abs}	Mg I 2852	Mg II 2796	Mg II 2803	Al II 1670	Al III 1854	Al III 1862	Si II 1526	Si II 1808	Ca II 3933	Ca II 3969	Cr II 2056
Q0005+0524	0.8514	201±19	1104±32	976±29	-	171±20	104±17	-	-	-	-	<3
Q0012-0122	1.3862	69±9	1115±14	891±15	290±12	94±9	44±9	304±4	-	-	-	<3
Q0021+0104A	1.3259	206±31	2727±28	2370±37	1038±40	-	-	880±47	<12	-	-	<6
Q0021+0104B	1.5756	459±61	3010±60	2468±71	-	<9	<6	1106±54	<5	-	-	<15
Q0427-1302	1.4080	-	316±8	225±7	61±5	<3	-	-	-	-	-	<3
Q1631+1156	0.9004	257±41	1081±29	908±38	-	-	-	-	-	133±34	-	<17
Q2051+1950	1.1157	454±23	1528±13	1448±11	747±37	392±18	-	-	105±33	300±27	-	44±11
Q2352-0028A	0.8730	85±28	1403±26	1075±36	-	-	-	-	-	<9	-	<9
Q2352-0028B	1.0318	445±29	2069±18	1984±16	-	809±40 ^c	189±22	-	170±24	-	-	<6
Q2352-0028C	1.2467	247±46	2975±28	2342±55	711±28	374±24	229±22	-	<5	-	-	<6
QSO	z_{abs}	Mn II 2576	Mn II 2594	Mn II 2606	Fe II 2260	Fe II 2344	Fe II 2374	Fe II 2382	Fe II 2586	Fe II 2600	Zn II ^a 2026	Zn II ^b 2062
Q0005+0524	0.8514	<3	<2	<3	<3	233±10	98±12	382±8	179±10	417±12	<3	<4
Q0012-0122	1.3862	<6	<7	<7	<10	330±8	187±6	460±18	-	460±15	<3	<4
Q0021+0104A	1.3259	<18	-	-	<16	1261±47	571±57	1829±42	1106±54	1836±59	<6	<7
Q0021+0104B	1.5756	<10	<13	<14	<22	1181±55	518±49	1873±69	982±41	1766±31	<16	<16
Q0427-1302	1.4080	<10	<10	-	<6	90±7	38±6	168±6	85±5	173±5	<3	<3
Q1631+1156	0.9004	<74	-	-	<7	-	-	617±21	400±28	624±78	<28	<25
Q2051+1950	1.1157	312±29	269±39	152±21	98±13	1118±15	831±32	1211±42	1154±16	1316±26	152±27	108±25
Q2352-0028A	0.8730	-	<5	-	<5	181±32	<5	362±15	78±12	266±12	<8	<15
Q2352-0028B	1.0318	-	<12	-	69±19	1362±9	761±20	1537±12	1304±16	1553±15	<18	<15
Q2352-0028C	1.2467	<11	-	-	<13	637±40	216±51	1151±50	508±56	936±37	<6	<5

^aThis line is a blend with Mg I λ 2026, although the Mg I contribution is judged to be insignificant in all cases.^bAs this line is blended with the Cr II λ 2062 line, this value represents the total EW of the line.^cBlended with another feature.

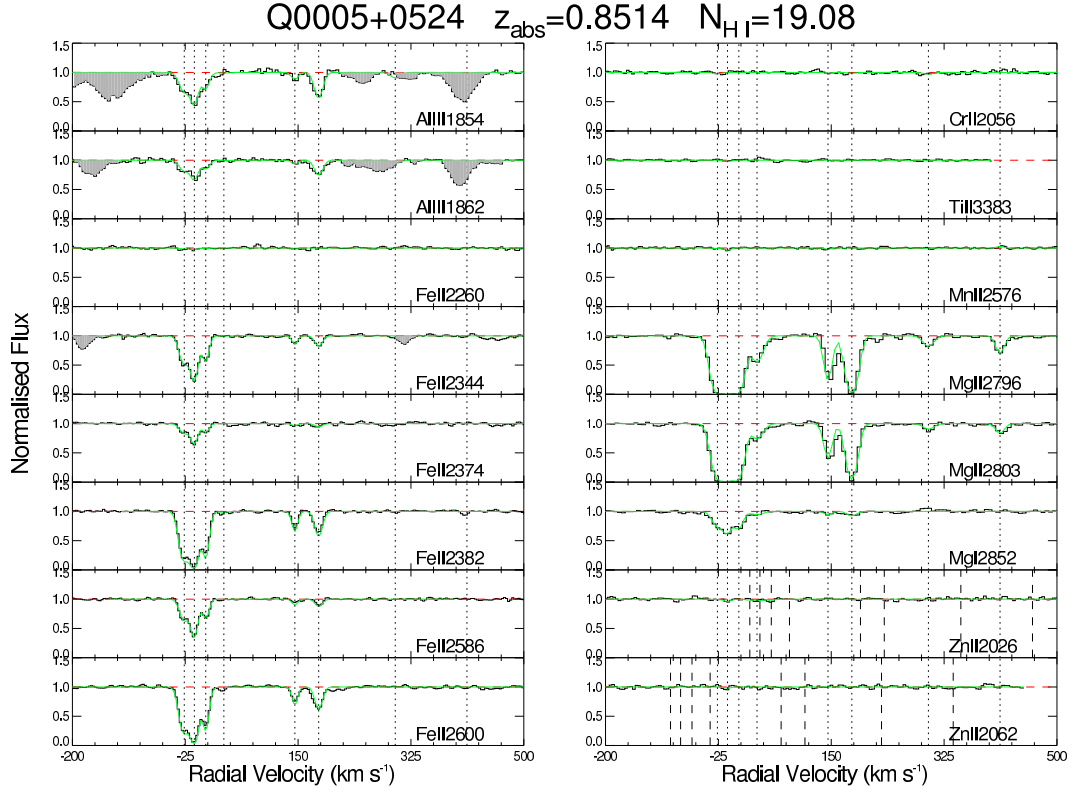


Figure 1. Velocity plots for Q0005+0524. The solid green line indicates the theoretical profile fit to the spectrum, and the dashed red line is the continuum level. The vertical dotted lines indicate the positions of the components that were used in the fit. In the cases of the Zn II $\lambda\lambda$ 2026,2062 lines, the long dashed vertical lines indicate the positions of the components for Mg I (former case), and Cr II (latter case). Areas shaded in gray are due to interloping absorption features or cosmetic defects.

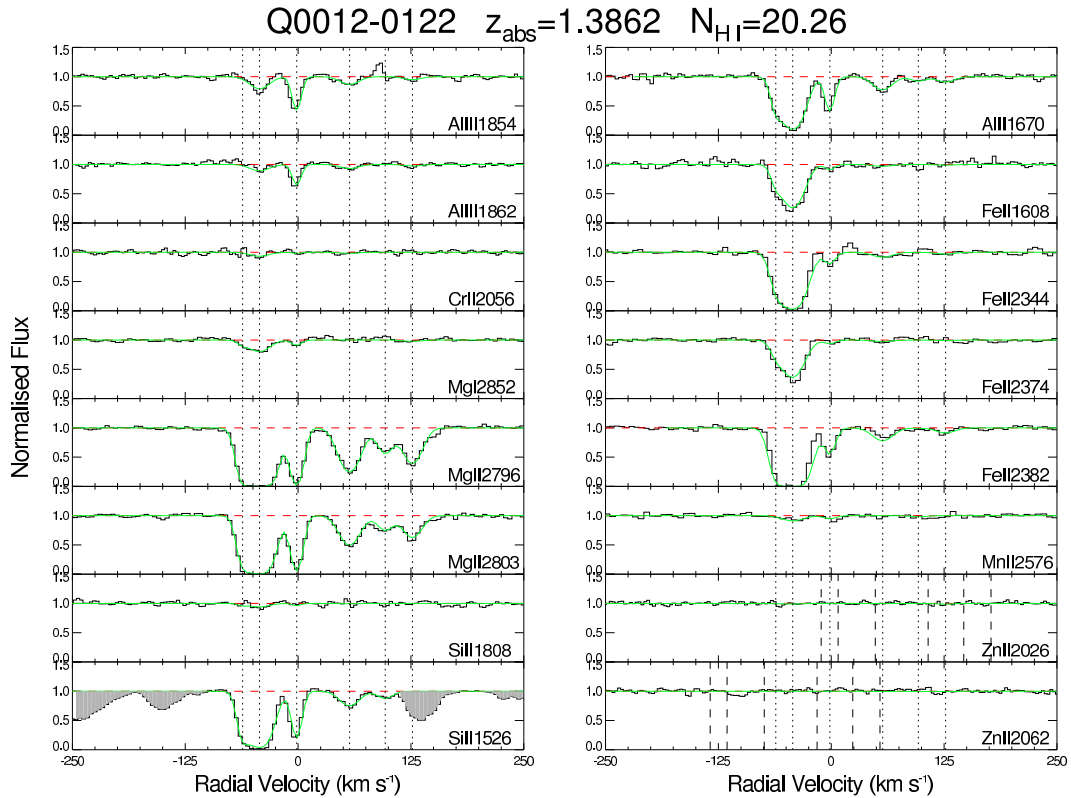


Figure 2. Same as Figure 1 but for Q0012-0122

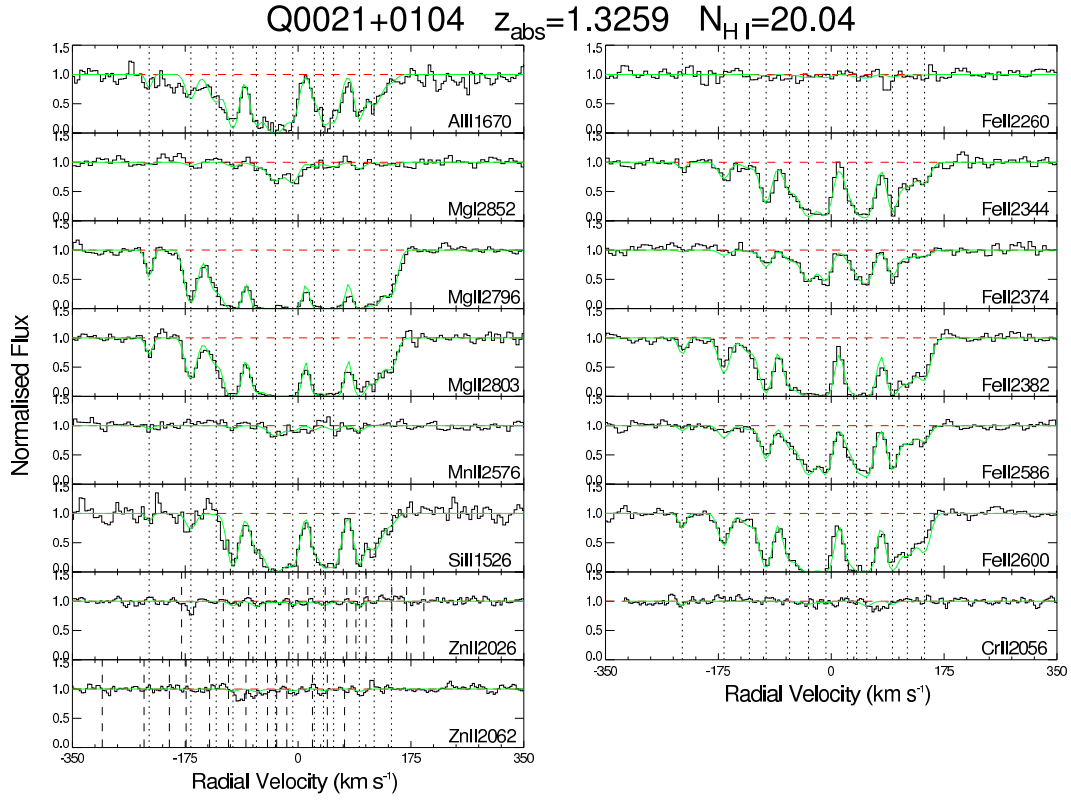


Figure 3. Same as Figure 1 but for Q0021+0104A

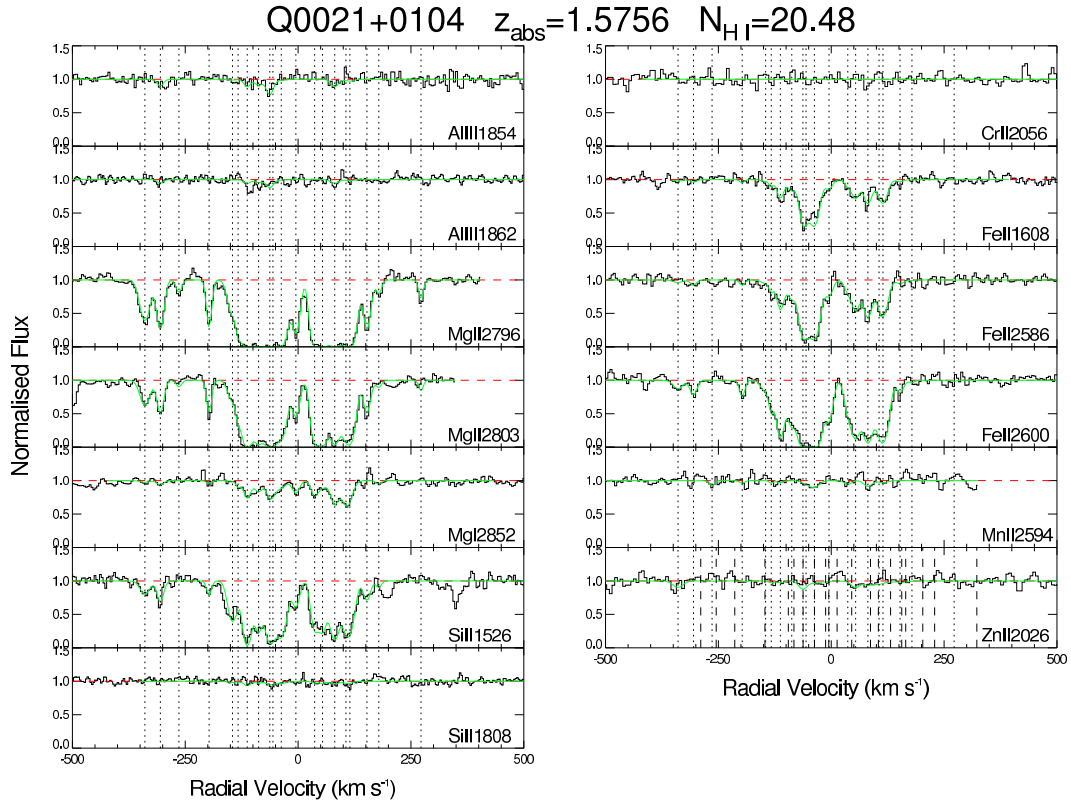


Figure 4. Same as Figure 1 but for Q0021+0104B

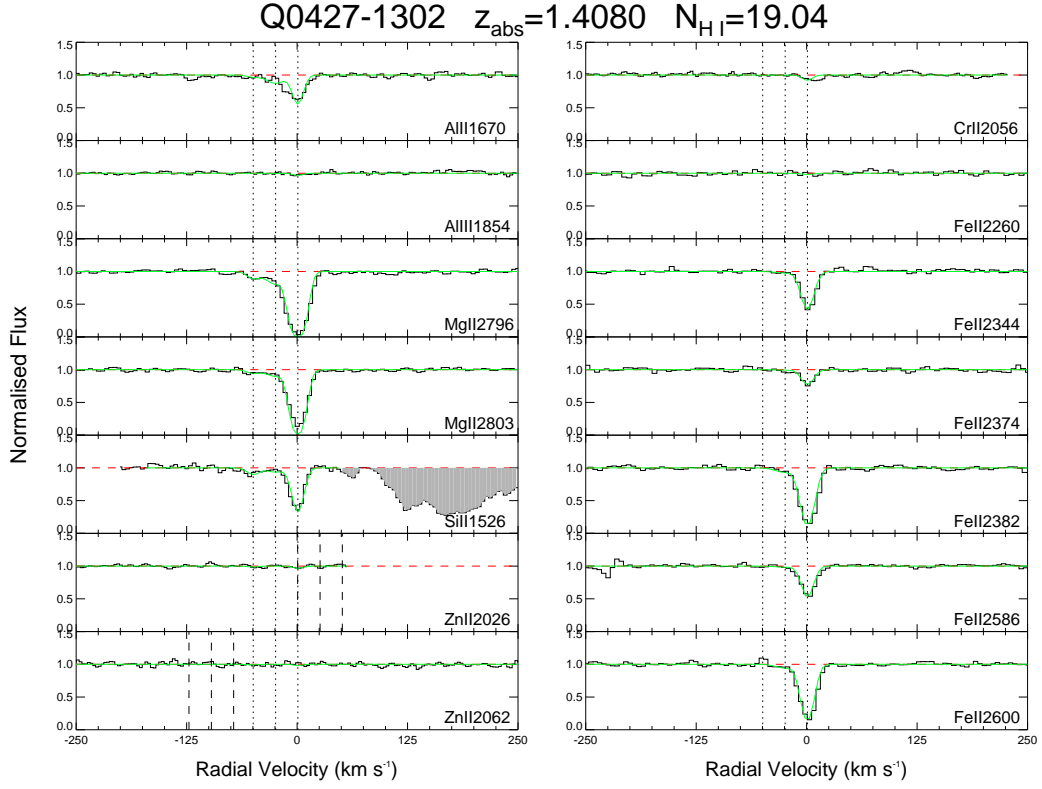


Figure 5. Same as Figure 1 but for Q0427-1302

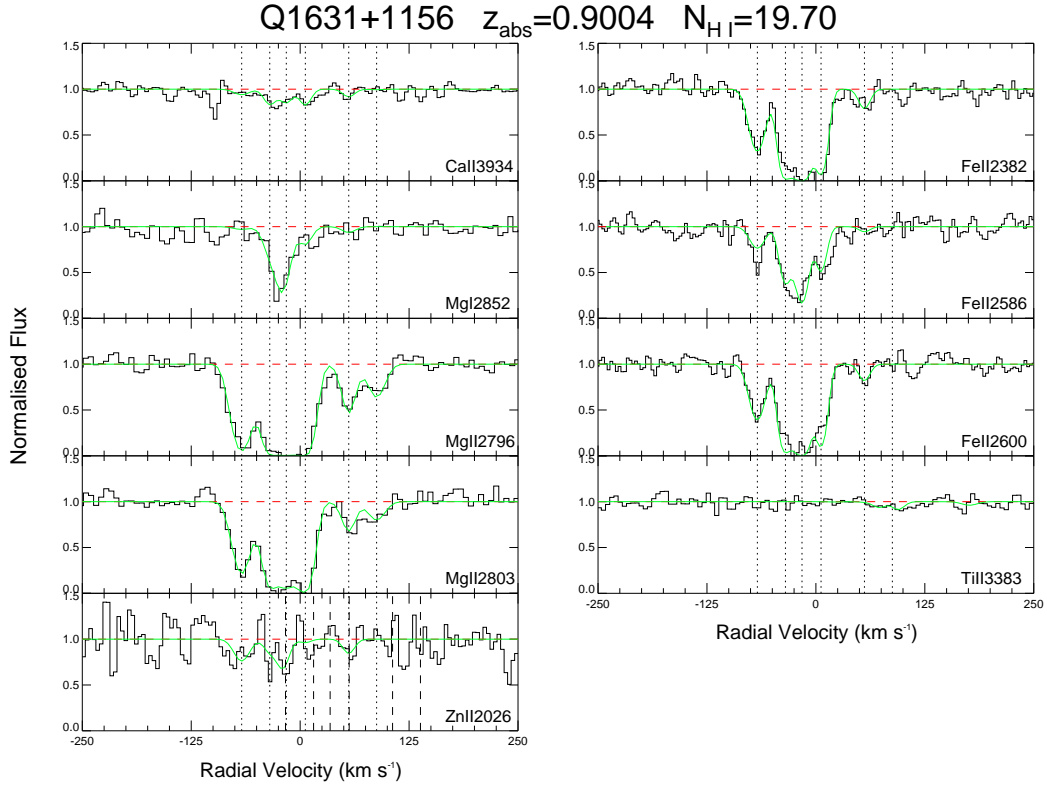


Figure 6. Same as Figure 1 but for Q1631+1156

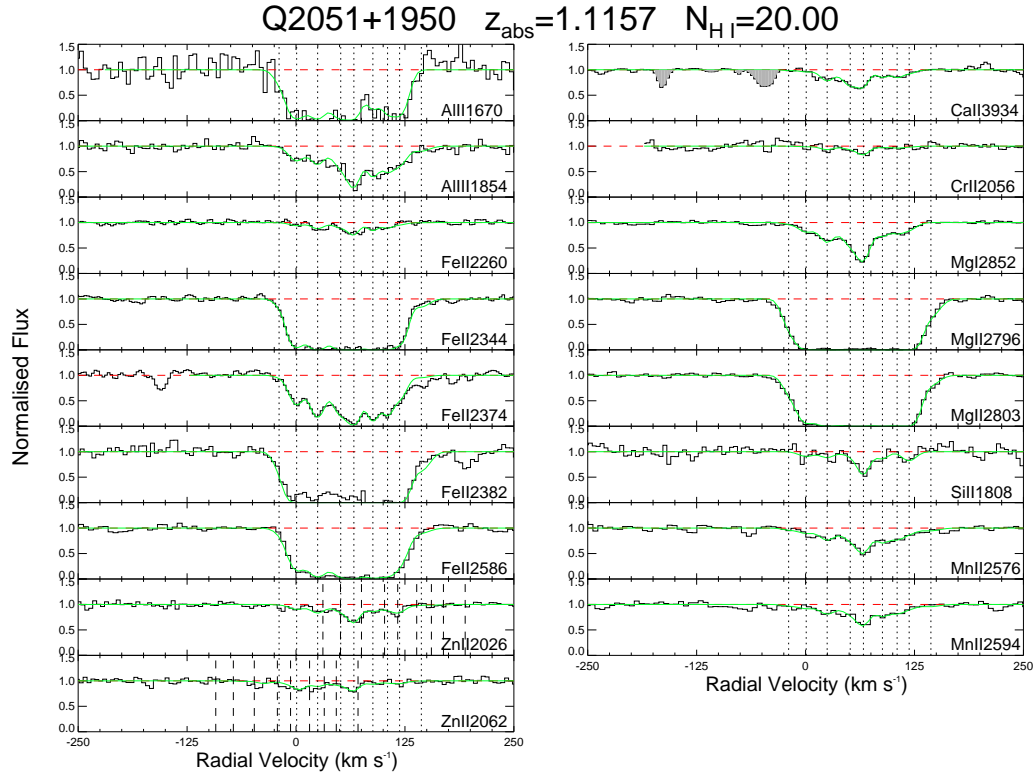


Figure 7. Same as Figure 1 but for Q2051+1950

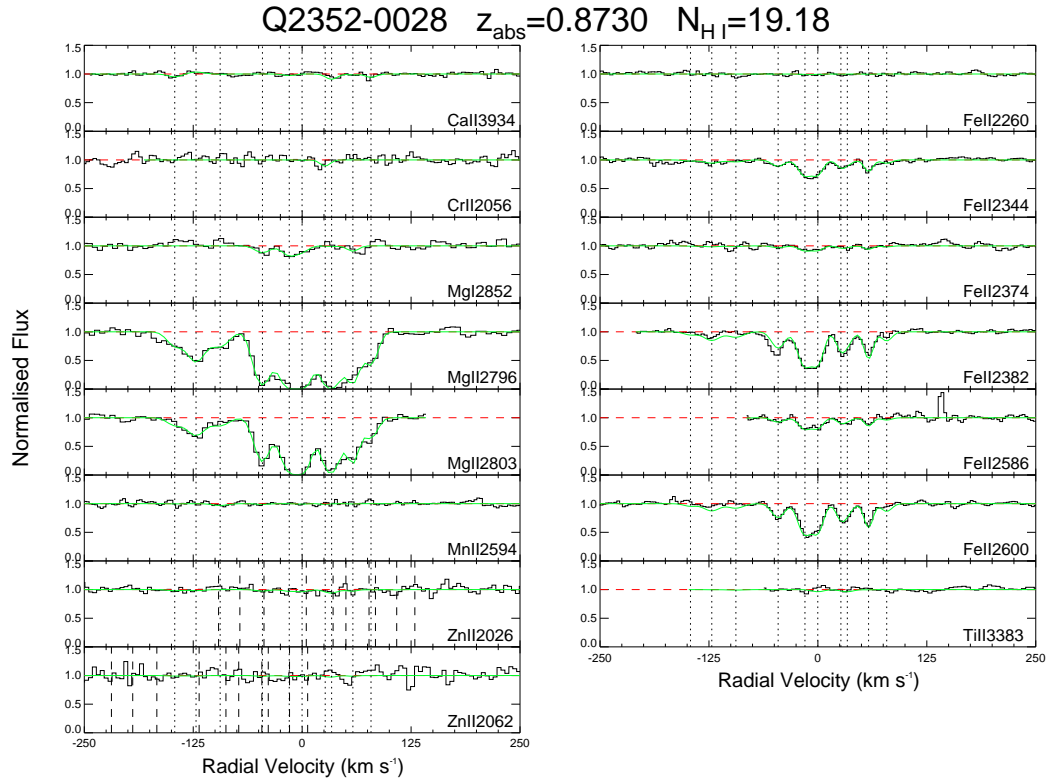


Figure 8. Same as Figure 1 but for Q2352-0028A

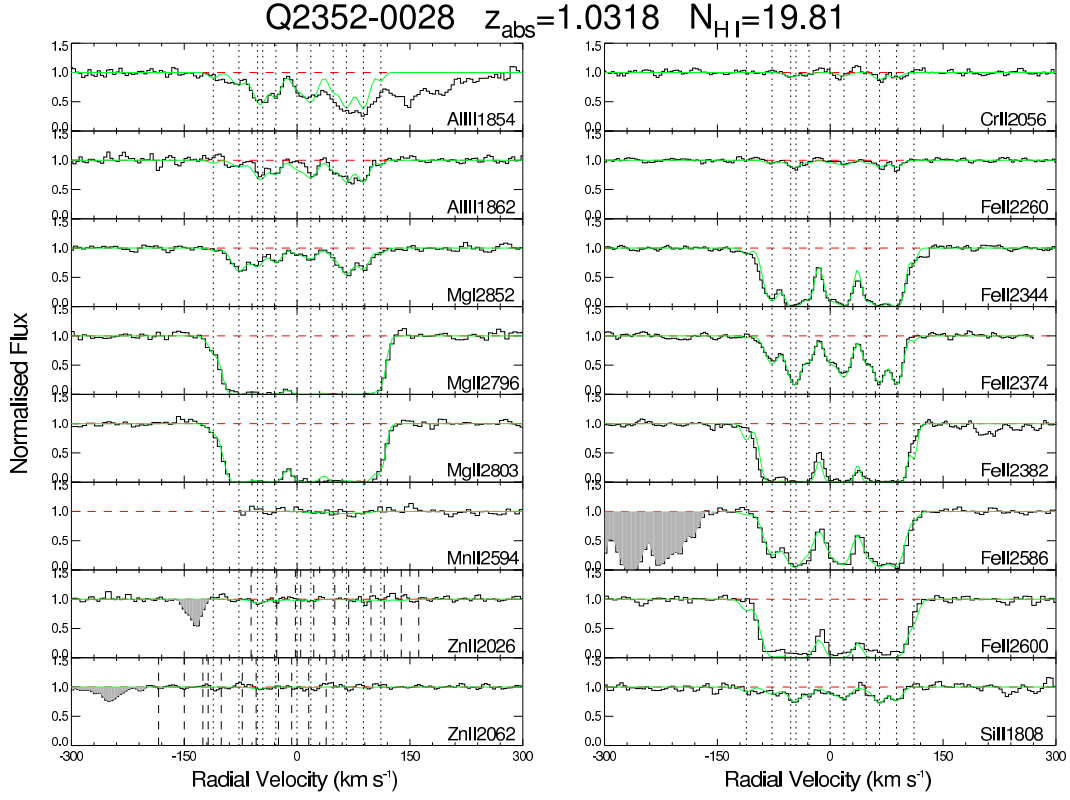


Figure 9. Same as Figure 1 but for Q2352-0028B

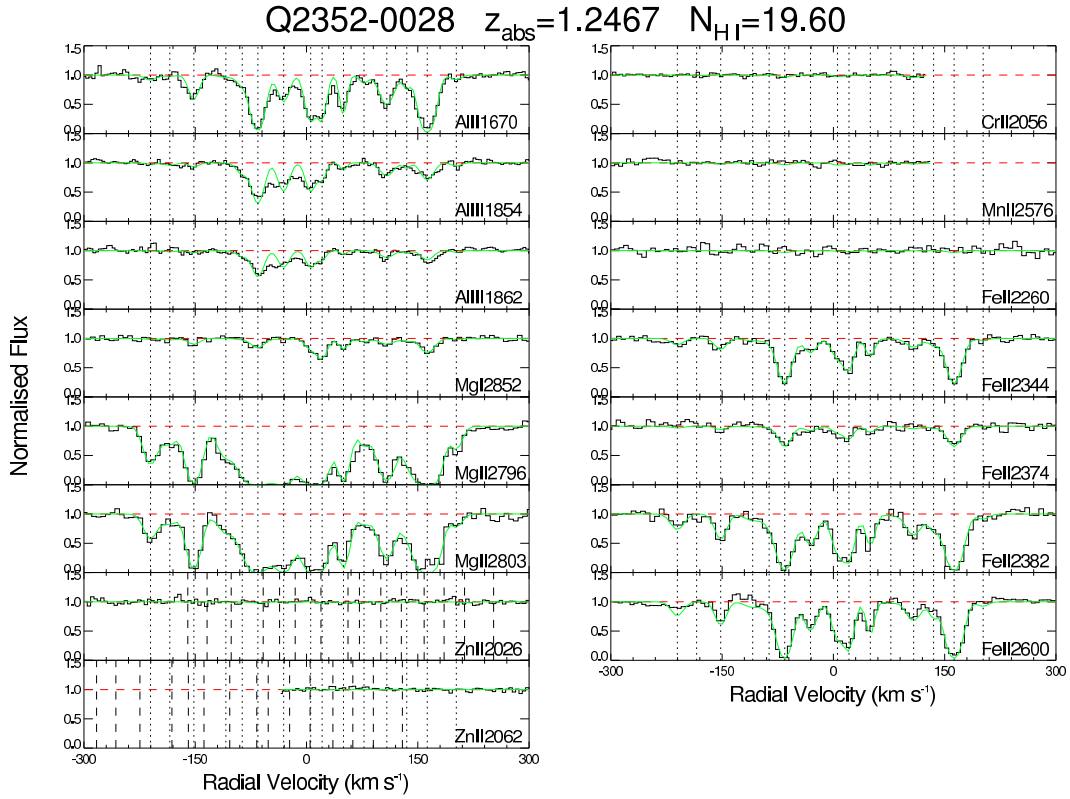


Figure 10. Same as Figure 1 but for Q2352-0028C

$[\text{Fe}/\text{H}] = -1.34 \pm 0.15$, typical of other DLA values in this redshift range. No Zn II $\lambda\lambda$ 2026, 2062 lines were detected in this system, and an upper limit of $[\text{Zn}/\text{H}] < -1.16$ was placed on the system. The Si II λ 1526 line was detected, although saturated. We derived a Si abundance for this system of $[\text{Si}/\text{H}] = -1.14$, which is consistent with the non-detection of the Si II λ 1808 line. This system shows weak α enhancement with $[\text{Si}/\text{Fe}] = +0.20$, although this could also be due to differential dust depletion. Kinematically, this system has an interesting absorption profile with two strong clusters of components separated by $\sim 100 \text{ km s}^{-1}$, possibly indicating a merging system. Velocity plots of several lines are shown in Figure 4.

4.0.4 Q0427-1302 ($z_{\text{em}} = 2.166$)

(System A: $z_{\text{abs}} = 1.4080$): This is a weak sub-DLA system with $\log N_{\text{H I}} = 19.04$ (Rao, Turnshek, & Nestor 2006). Only three components were used in the fit, with the vast majority of the absorption in the $v \sim 0 \text{ km s}^{-1}$ component. We detected lines of Mg II $\lambda\lambda$ 2796, 2803, Al II λ 1670, Si II λ 1526, and Fe II $\lambda\lambda$ 2344, 2374, 2382, 2586, 2600. This system is metal poor, with $[\text{Fe}/\text{H}] = -1.12 \pm 0.04$. No Zn II $\lambda\lambda$ lines were detected with $S/N \sim 55$ in the region, and an upper limit of $[\text{Zn}/\text{H}] < -0.58$ was placed on the system. The Al III $\lambda\lambda$ 1854, 1862 lines were covered but not detected. An upper limit was placed on the Al III/Al II ratio of $\text{Al III}/\text{Al II} < -1.14$. This system also shows slight α enhancement with $[\text{Si}/\text{Fe}] = +0.16 \pm 0.03$. Velocity plots of several lines are shown in Figure 5.

4.0.5 Q1631+1156 ($z_{\text{em}} = 1.792$)

(System A: $z_{\text{abs}} = 0.9004$): This system is a sub-DLA with $\log N_{\text{H I}} = 19.70$ (Rao, Turnshek, & Nestor 2006). The Fe II $\lambda\lambda$ 2344, 2374 lines were affected by a cosmetic defect in the chip, but the Fe II $\lambda\lambda$ 2382, 2586, 2600 lines were detected. Other lines detected were Mg I λ 2852, Mg II $\lambda\lambda$ 2796, 2803, and Ca II 3934. The Zn II $\lambda\lambda$ 2026, 2062 lines were covered but not detected, with $S/N \sim 6$ in the region. Six components were used in the profile fits. We determined the metallicity for this system based on Fe to be $[\text{Fe}/\text{H}] = -1.06 \pm 0.06$, and based on Zn, $[\text{Zn}/\text{H}] < -0.15$. Velocity plots of several lines are shown in Figure 6.

4.0.6 Q2051+1950 ($z_{\text{em}} = 2.367$)

(System A: $z_{\text{abs}} = 1.1157$): Although Rao, Turnshek, & Nestor (2006) determined $\log N_{\text{H I}} = 19.26$ for this object, we refit the UV STIS spectrum for this object to determine $\log N_{\text{H I}} = 20.00 \pm 0.15$. Even with this substantially higher $N_{\text{H I}}$ value, this object appears to have super solar metallicity. We detected lines of Mg I λ 2852, Mg II $\lambda\lambda$ 2796, 2803, Al III $\lambda\lambda$ 1854, Si II λ 1808, Cr II λ 2056, Mn $\lambda\lambda$ 2576, 2594, 2606, Fe II $\lambda\lambda$ 2260, 2344, 2374, 2382, 2586, 2600, and Zn II $\lambda\lambda$ 2026, 2062. Nine components were used in the profile fits. The Al II λ 1670 line is heavily saturated, so only a lower limit could be placed on the column density. The Al III/Al II ratio for this system is $\text{Al III}/\text{Al II} < -0.17$. The Ca II λ 3934 line is clearly detected, with $W_0(3934) = 133 \pm 34$

mÅ. This system shows strong Fe II absorption features, with $[\text{Fe}/\text{H}] = -0.45 \pm 0.15$, much higher than typical DLA systems. We also detect Zn II $\lambda\lambda$ 2026, 2062 at $> 5\sigma$, with $[\text{Zn}/\text{H}] = +0.27 \pm 0.18$. This system has moderate dust depletion with $[\text{Zn}/\text{Fe}] = +0.72 \pm 0.10$. Manganese is also slightly overabundant relative to Fe in this system, with $[\text{Mn}/\text{Fe}] = +0.16 \pm 0.03$. Velocity plots of several lines are shown in Figure 7.

4.0.7 Q2352-0028 ($z_{\text{em}} = 1.628$)

(System A: $z_{\text{abs}} = 0.8739$): This is a weak sub-DLA system with $\log N_{\text{H I}} = 19.18$ (Rao, Turnshek, & Nestor 2006). 10 components were used in the profile fits. We detect lines of Mg I λ 2852, Mg II $\lambda\lambda$ 2796, 2803, and Fe II $\lambda\lambda$ 2344, 2382, 2586, 2600. The Ti II λ 3383 line was covered, but was not detected. This is not unsurprising as this line is weak in most systems. The Al II λ 1670 and Al III $\lambda\lambda$ 1854, 1862 lines were below the covered wavelengths and could not be measured. The Zn II $\lambda\lambda$ 2026, 2062 lines were not detected at $S/N \sim 20$ in the region. This system has a low metallicity, with $[\text{Fe}/\text{H}] = -1.17 \pm 0.9$, and $[\text{Zn}/\text{H}] < -0.14$. Velocity plots of several lines are shown in Figure 8.

(System B: $z_{\text{abs}} = 1.0318$): This is a sub-DLA system with $\log N_{\text{H I}} = 19.81$ (Rao, Turnshek, & Nestor 2006). 11 components were used in the profile fitting analysis. Lines of Mg I λ 2852, Mg II $\lambda\lambda$ 2796, 2803, Al III $\lambda\lambda$ 1854, 1862, Si II λ 1808 and Fe II $\lambda\lambda$ 2260, 2344, 2374, 2382, 2586, 2600. The Al III λ 1854 was partially blended with an interloping feature, but the weaker Al III λ 1862 was unperturbed. The Al II λ 1670 line lies just below the accessible wavelengths and was not covered. This system has a moderate value of $\text{Fe II}/\text{Al III} = +1.50 \pm 0.03$. This sub-DLA has a high metallicity, with $[\text{Fe}/\text{H}] = -0.37 \pm 0.13$. Based on Si the metallicity is $[\text{Si}/\text{H}] = +0.14 \pm 0.14$. The Zn II $\lambda\lambda$ 2026, 2062 lines were not detected at $S/N \sim 30$ in the region, giving an upper limit on the Zn abundance as $[\text{Zn}/\text{H}] < -0.51$. This system shows signs of moderate α enhancement with $[\text{Si}/\text{Fe}] = +0.51 \pm 0.03$. Velocity plots of several lines are shown in Figure 9.

(System C: $z_{\text{abs}} = 1.2467$): This system is a sub-DLA with $\log N_{\text{H I}} = 19.60$ (Rao, Turnshek, & Nestor 2006). The complex absorption profile required 15 components to properly fit the system. We detected lines of Mg I λ 2852, Mg II $\lambda\lambda$ 2796, 2803, Al II λ 1670, Al III $\lambda\lambda$ 1854, 1862, and Fe II $\lambda\lambda$ 2344, 2374, 2382, 2586, 2600. This sub-DLA appears to have significant amounts of ionisation with $\text{Al III}/\text{Al II} = -0.10 \pm 0.03$ and $\text{Fe II}/\text{Al III} = +0.82 \pm 0.03$. The Zn II $\lambda\lambda$ 2026, 2062 lines were not detected with $S/N \sim 30$ in the region. We placed an upper limit of $[\text{Zn}/\text{H}] < -0.70$ for this system. Based on the Fe II lines, this system has a metallicity of $[\text{Fe}/\text{H}] = -0.86 \pm 0.24$. Velocity plots of several lines are shown in Figure 10.

5 [MN/FE] - NUCLEOSYNTHETIC EFFECTS

Mn and Fe are an interesting pair of elements to study in QSO absorbers for reasons discussed below, and has been investigated in the past by several groups (Pettini et al. 2000; Dessauges-Zavadsky, Prochaska, & D’Odorico 2002; Ledoux, Bergeron, & Petitjean 2002). The lines of Mn II $\lambda\lambda$ 2576, 2594, 2606 are usually simultaneously accessible

QSO	z_{abs}	$\log N_{\text{H I}}$	Mg I	Mg II	Al II	Al III	Si II	Ca II	Ti II	Cr II	Mn II	Fe II	Zn II
Q0005+0524	0.8514	19.08±0.04	12.18±0.02	>14.32	-	13.11±0.04	-	-	<11.03	<11.88	<11.01	13.79±0.01	<11.24
AOD			12.24±0.04	>14.13		13.13±0.06						13.75±0.02	
Q0012-0122	1.3862	20.26±0.02	11.73±0.03	>14.09	>13.08	12.89±0.02	14.43±0.08	-	<11.96	<11.89	<11.41	14.24±0.01	<11.55
AOD			11.75±0.05	>13.81	>13.07	12.83±0.04	14.45±0.04					14.25±0.01	
Q0021+0104A	1.3259	20.04±0.11	12.16±0.04	>14.86	>13.71	-	>14.90	-	-	<12.21	<11.87	14.69±0.01	<11.48
AOD			12.26±0.06	>14.50	>13.68		>14.86					14.68±0.04	
Q0021+0104B	1.5756	20.48±0.15	12.61±0.03	>14.57	-	12.26±0.08	14.88±0.03	-	-	<12.58	<11.90	14.61±0.02	<11.95
AOD			12.60±0.06	>14.51		12.31±0.17	14.86±0.02					14.58±0.02	
Q0427-1302	1.4080	19.04±0.04	-	>13.74	12.20±0.03	<11.06	13.59±0.03	-	-	<11.87	<11.65	13.36±0.01	<11.09
AOD				>13.25	12.21±0.03		13.56±0.04					13.33±0.02	
Q1631+1156	0.9004	19.70±0.04	12.35±0.06	>14.18	-	-	-	12.13±0.07	<11.66	<12.65	<12.54	14.11±0.02	<12.18
AOD			12.44±0.05	>14.04				12.22±0.10				14.17±0.03	
Q2051+1950	1.1157	20.00±0.15	12.64±0.02	>14.61	>13.70	13.53±0.03	15.15±0.07	12.55±0.04	-	12.89±0.10	13.21±0.02	15.02±0.02	12.90±0.10
AOD			12.67±0.02	>14.44	>13.77	13.52±0.02	15.31±0.12	12.59±0.04		13.08±0.10	13.24±0.04	15.00±0.02	12.97±0.07
Q2352-0028A	0.8730	19.18±0.09	11.85±0.06	>14.27	-	-	-	<11.01	<11.36	<12.37	<11.46	13.48±0.02	<11.67
AOD			11.84±0.14	>14.05								13.47±0.02	
Q2352-0028B	1.0318	19.81±0.13	12.53±0.02	>14.94	-	13.41±0.02	15.49±0.03	-	-	12.96±0.06	<11.87	14.91±0.01	<11.93
AOD			12.60±0.03	>14.58		13.41±0.05	15.49±0.06			12.94±0.26		14.88±0.01	
Q2352-0028C	1.2467	19.60±0.24	12.33±0.02	>15.24	13.49±0.02	13.39±0.02	-	-	-	<12.17	<11.60	14.21±0.01	<11.53
AOD			12.32±0.07	>14.39	13.42±0.02	13.43±0.03						14.19±0.09	

Table 3: Total column densities from the absorbers in this sample.

QSO	z_{abs}	$\log N_{\text{H I}}$	[Zn/H]	[Fe/H]	[Fe/Zn]	[Si/Fe]	[Ca/Fe]	[Cr/Fe]	[Mn/Fe]	Al III / Al II	Mg II / Mg I	Mg II / Al III	Fe II / Al III
[X/Y] _⊙			-7.37	-4.53	+2.84	+0.07	-1.13	-1.82	-1.97				
Q0005+0524	0.8514	19.08±0.04	< -0.47	-0.76±0.05	> -0.29	-	-	< -0.09	< -0.81	-	>2.14	>+1.21	0.68±0.04
Q0012-0122	1.3862	20.26±0.02	< -1.34	-1.49±0.03	> -0.15	+0.12±0.08	-	< -0.53	< -0.86	< -0.19	>2.36	>+1.20	1.35±0.03
Q0021+0104A	1.3259	20.04±0.11	< -1.19	-0.82±0.11	> +0.37	>+0.14	-	< -0.66	< -0.85	-	>2.70	-	-
Q0021+0104B	1.5756	20.48±0.15	< -1.16	-1.34±0.15	> -0.18	+0.20±0.04	-	< -0.21	< -0.74	-	>1.96	>+2.31	2.35±0.08
Q0427-1302	1.4080	19.04±0.04	< -0.58	-1.15±0.04	> -0.57	+0.16±0.03	-	< +0.33	< +0.26	< -1.14	-	-	>2.30
Q1631+1156	0.9004	19.70±0.04	< -0.15	-1.06±0.06	> -0.91	-	-0.85±0.07	< +0.36	< +0.40	-	>1.83	-	-
Q2051+1950	1.1157	20.00±0.15	+0.27±0.18	-0.45±0.15	-0.72±0.10	+0.06±0.07	-1.34±0.05	-0.31±0.10	+0.16±0.03	< -0.17	>1.97	>+1.08	1.49±0.04
Q2352-0028A	0.8730	19.18±0.09	< -0.14	-1.17±0.09	> -1.03	-	< -1.34	< +0.71	< -0.05	-	>2.42	-	-
Q2352-0028B	1.0318	19.81±0.13	< -0.51	-0.37±0.13	> +0.14	+0.51±0.03	-	-0.13±0.06	< -1.07	-	>2.41	>+1.53	1.50±0.03
Q2352-0028C	1.2467	19.60±0.24	< -0.70	-0.86±0.24	> -0.16	-	-	< -0.22	< -0.64	-0.10 ± 0.03	>2.91	>+1.85	0.82±0.03

Table 4: Abundances and adjacent ion ratios for the absorbers in this sample.

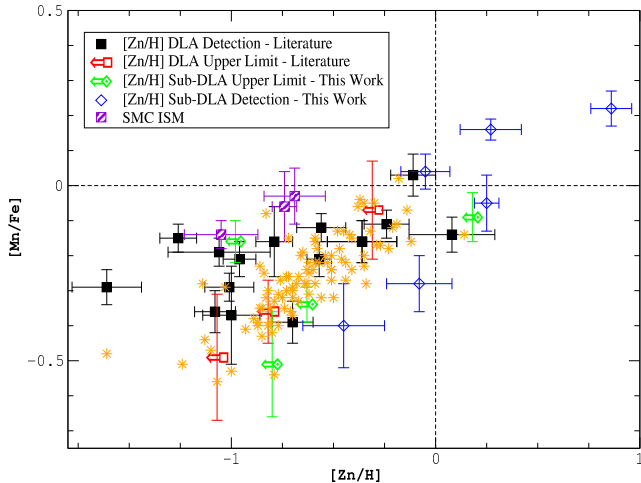


Figure 11. $[\text{Mn}/\text{Fe}]$ vs. $[\text{Zn}/\text{H}]$ for sub-DLAs, as well as the DLAs with Mn and Fe detections from the literature. The star shaped orange points are Milky Way stellar abundances from Reddy, Lambert & Prieto (2006). The sub-DLA points are from these measurements as well as Meiring et al. (2007, 2008). Also shown are the ISM abundances for the SMC from Welty et al. (2001)

with Fe II lines with the MIKE spectrograph due to the large wavelength coverage available. In Milky Way stars, the Mn abundance seems to have a strong metallicity dependence. A clear trend between $[\text{Mn}/\text{Fe}]$ and $[\text{Fe}/\text{H}]$ in the sense that $[\text{Mn}/\text{Fe}]$ increases to near solar values as $[\text{Fe}/\text{H}]$ increases also is seen (McWilliam, Rich & Smecker-Hane 2003; Nissen et al. 2000; Gratton et al. 2004). This seems to indicate that the nucleosynthetic origin of Mn is in Type Ia supernovae, as with the α -capture elements which are produced in Type II SNe, $[\alpha/\text{Fe}]$ tends to decrease with increasing $[\text{Fe}/\text{H}]$. Samland (1998) argue that $\sim 75\%$ of Mn is produced in Type Ia supernovae explosions. On the other hand, Timmes, Woosley, & Weaver (1995) suggest that metallicity dependent yields in Type II supernovae can also reproduce the observed trends. Feltzing, Fohlman & Bensby (2007) favor metallicity dependent yields with Type II SNe as the major contributors based on their observations of stellar abundances in the Milky Way and a compilation of other stellar abundances, but note that the Type Ia enrichment scenario is impossible to rule out.

Whatever the underlying production mechanism of Mn may be, there does seem to be a trend between $[\text{Mn}/\text{Fe}]$ and metallicity. As the condensation temperatures of Mn and Fe are similar, and accordingly have similar levels of depletion especially in the warm and halo ISM of the Milky Way, the relative abundances of these two elements are expected to be mainly nucleosynthetic in origin.

In Figure 11 we show $[\text{Mn}/\text{Fe}]$ vs. $[\text{Zn}/\text{H}]$ for these absorbers, as well as ones taken from the literature. Overlaid on the same graph are the data points from Reddy, Lambert & Prieto (2006) from Milky Way stars, and the interstellar abundances from Welty et al. (2001). A clear trend of increasing $[\text{Mn}/\text{Fe}]$ with increasing $[\text{Zn}/\text{H}]$ is seen, as is seen in the Milky Way. A Spearman rank correlation coefficient for these data was determined to be $r_s = 0.497$ with a probability of obtaining this value by chance of 0.003.

Kendall's τ was also determined to be $\tau = 0.359$, with a probability of no correlation also of 0.003. The absorber sample has a larger dispersion than the stellar abundances from Reddy, Lambert & Prieto (2006), which is possibly a result of the combined effects of some differential depletion between Mn and Fe, and the fact that the galaxies sampled via absorption lines are likely from a mixture of morphological types. The two sub-DLA points in Figure 11 that lie below the stellar points at $([\text{Zn}/\text{H}], [\text{Mn}/\text{Fe}]) \sim (-0.5, -0.4)$ and $(-0.1, -0.3)$ also have the largest associated errors in $[\text{Mn}/\text{Fe}]$, but are well within $\sim 2\sigma$ of the stellar abundances. The apparent optical depth and profile fitting column density determinations of Zn II in these systems agree within the error bars.

We note that the relative abundance ratio of $[\text{Mn}/\text{Fe}]$ does not appear to be significantly altered by ionisation effects for reasonable estimates of the ionisation parameter (Dessauges-Zavadsky, Prochaska, & D'Odorico 2002; Meiring et al. 2008). A similar trend was seen in Ledoux, Bergeron, & Petitjean (2002) for $[\text{Mn}/\text{Fe}]$ as well, albeit with a smaller sample size.

6 DISCUSSION

Total ionic column densities are given in Table 3. The abundances for the observed systems are given in Table 4, where we have used the total column densities (i.e. the sum of the column densities in the individual components of a system that were determined via profile fitting method) along with the total $N_{\text{H I}}$ as given in Table 2, to determine the abundances of these systems. We have not assumed any ionisation corrections on these abundances, and have assumed the first ions to be the dominant ionisation species of the elements for which these abundances have been determined, namely Zn, Fe, Mn, Cr, and Si. Solar systems abundances from Lodders (2003) are also given in Table 4.

Relative abundances of various elements are also given in Table 4, with the column densities also determined from the profile fitting analysis. Along with the metallicities, we give the ratio $[\text{Zn}/\text{Fe}]$, which is often used as an indicator of dust depletion. We also provide the ratios of $[\text{Si}/\text{Fe}]$, $[\text{Ca}/\text{Fe}]$, $[\text{Cr}/\text{Fe}]$, and $[\text{Mn}/\text{Fe}]$. Finally, we provide ratios of the column densities of the adjacent ions Al III/Al II and Mg II/Mg I as well as Mg II/Al III and Fe II/Al III, any of which may provide information about the ionisation in these systems. Photoionization modeling has shown that the ionisation corrections necessary are small in most cases, with correction terms comparable to the individual errors on the abundances (Dessauges-Zavadsky et al. 2003; Prochaska et al. 2006; Meiring et al. 2007, 2008).

The trend of a rising ratio in $[\text{Mn}/\text{Fe}]$ with increasing metallicity for QSO absorbers, both DLAs and sub-DLAs, mimics the trend seen in Milky Way stars. A similar comparison with stellar abundances from the SMC and LMC could also shed light on the morphological types of the absorber host galaxies, as the Magellanic clouds have undergone much different star formation histories than the Milky Way (Pagel & Tautvaisiene 1998; Carrera et al. 2008).

Similarly, the $[\text{Mn}/\text{Fe}]$ ratio would be interesting to study in detail for a large number of systems over a large redshift range as was done for small

samples in Dessauges-Zavadsky, Prochaska, & D’Odorico (2002); Ledoux, Bergeron, & Petitjean (2002). Due to the intrinsic scatter in the data, a large statistical sample is needed to investigate [Mn/Fe] vs. z . The Mn II triplet at ~ 2600 Å is however difficult to detect at $z > 1.75$ as these lines are sometimes blended with telluric features at these redshifts. On the other hand, these lines can be probed with ground based spectra at $z \gtrsim 0.25$.

It would be interesting to see if the [Mn/Fe] ratio plateaus to a constant value of [Mn/Fe] ~ -0.4 dex as seen in metal poor stars with [Fe/H] $\lesssim -1.5$ (Bai et al. 2004; McWilliam, Rich & Smecker-Hane 2003). Also, [Mn/O] would be an interesting abundance ratio to study as O is almost solely produced in Type II SNe, and Fe is produced in both Type Ia and Type II explosions. [Mn/O] vs [O/H] for dwarf spheroidals and the Milky Way show quite distinct trends (see for instance Feltzing, Fohlman & Bensby 2007), and as such may shed light on the morphology of these absorption systems. With these elements however, the task of separating the differential dust depletion between Mn and O and true nucleosynthetic differences may be difficult.

Here, we have presented rest frame equivalent widths, column densities, and abundances for these 10 absorbers based on spectra taken with the MIKE spectrograph. Zn, the preferred metallicity indicator, is detected in only one system (the $z_{abs}=1.1157$ system in Q2051+1950), so an estimate of the mean metallicity based on Zn from survival analysis is impossible as survival analysis requires a higher fraction of detections for an accurate estimate of the mean.

Based on the more heavily depleted element Fe which is detected in all systems, the N_H -weighted mean metallicity is $\langle [Fe/H] \rangle = -0.77 \pm 0.11$. This is nearly 0.7 dex higher than what is seen in DLA systems at these redshifts, $\langle [Fe/H]_{DLA} \rangle \sim -1.5$, and even higher than the N_H -weighted mean metallicity based on Zn measurements for DLAs at these redshifts (see for instance Kulkarni et al. (2007) and references therein). In an forthcoming paper, we combine these values with those from our previous work in Meiring et al. (2007, 2008); Péroux et al. (2006b) to examine the full sample of high resolution sub-DLAs at $z < 1.5$ from our MIKE and UVES observations including kinematics, mean metallicities, and relative abundances.

ACKNOWLEDGMENTS

We thank the exceptionally helpful staff of Las Campanas Observatory for their assistance during the observing runs. Thanks to the anonymous referee for several helpful suggestions. J. Meiring and V.P. Kulkarni gratefully acknowledge support from the National Science Foundation grant AST-0607739 (PI Kulkarni). J. Meiring acknowledges partial support from a South Carolina Space Grant graduate student fellowship for a portion of this work.

REFERENCES

Bai G.S., Zhao G. Chen Y.Q., Shi J.R., Klochkova V.G., Panchuk V.E., Qiu H.M., Zhang H.W., 2004, *A&A*, 425, 671

Bernstein R., Schectman S.A., Gunnels S., Mochnacki S., Athey A., 2003 *SPIE*, 4841, 1694
 Bosma A., 1981, *AJ*, 86, 1825
 Cen R., Ostriker J.P., Prochaska J.X., Wolfe A.M., 2003, *ApJ*, 598, 741
 Carrera R., Gallart C., Aparicio A., Costa E., Méndez R.A., Noel N.E.D., 2008, *AJ*, 136, 1039
 Charlton J.C., Ding J., Zonak S.G., Churchill C.W., Bond N.A., Rigby J.R., 2003, *ApJ*, 589, 111
 Danforth C.W., Shull M.J., 2008, *ApJ*, 679, 194
 Dessauges-Zavadsky M., Prochaska J.X., D’Odorico S., 2002, *A&A*, 391, 801
 Dessauges-Zavadsky M., Péroux C., Kim T.S., D’Odorico S., McMahon R.G., 2003, *MNRAS*, 345, 447
 Ding J., Charlton J.C., Churchill C.W., Palma C., 2003, *ApJ*, 590, 746
 Ellison, S., 2006, *MNRAS*, 368, 355
 Feltzing S. Fohlman M., Bensby T., 2007, *A&A*, 2007, 467, 665
 Ferland G. J., Korista K.T., Verner D.A., Ferguson J.W., Kingdon J.B., Verner E.M., 1998, *PASP*, 110, 761
 Frank S., Mathur S., York D.G., 2008, *AJ*, submitted
 Gratton R.G., Caretta E., Claudi R., Lucatello S., Barbieri M., 2004, *A&A*, 404, 187
 Hewitt A., Burbidge G., 1987, *ApJS*, 63, 1
 Khare P., Kulkarni V.P., Lauroesch J.T., York D.G., Crotts P.S., Nakamura O., 2004, *ApJ*, 616, 86
 Khare P., Kulkarni V.P., Péroux C., York D.G., Lauroesch J.T., Meiring J.D., 2007, *A&A*, 464, 487
 Kulkarni V.P., Fall S.M., Lauroesch J.T., York D.G., Welty D.E., Khare P., Truran J.W., 2005, *ApJ*, 618, 68
 Kulkarni V.P., Khare P., Péroux C., York D.G., Lauroesch J.T., Meiring J.D., 2007, *ApJ*, 661, 88
 Ledoux C., Bergeron J., Petitjean P., 2002, *A&A*, 385, 802
 Lodders, K., 2003, *ApJ*, 591, 1220
 McWilliam A., Rich R.M., Smecker-Hane T.A., 2003, *ApJ*, 592, 21
 Meiring J.D., Kulkarni V.P., Khare P., Bechtold J., York D.G., Cui J., Lauroesch J.T., Crotts A.P.S., Nakamura O., 2006, *MNRAS*, 370, 43
 Meiring J.D., Lauroesch J.T., Kulkarni V.P., Péroux C., Khare P., York D.G., Crotts A.P.S., 2007, *MNRAS*, 376, 557
 Meiring J.D., Kulkarni V.P., Lauroesch J.T., Péroux C., Khare P., York D.G., Crotts A.P.S., 2008, *MNRAS*, 384, 1015
 Miller E.D., Knezek P.M., Bregman J.E., 1999, *ApJ*, 510, 95
 Morton D.C., 2003, *ApJS*, 149, 205
 Nissen P.E., Chen Y.Q., Schuster W.J., Zhao G., 2000, *A&A*, 353, 722
 Nissen P. E., Chen Y. Q., Asplund M., Pettini M., 2004, *A&A*, 415, 993
 Pagel B.E.J., Tautvaisiene G., 1998, *MNRAS*, 299, 535
 Péroux C., Storrie-Lombardi L., McMahon R., Irwin M., & Hook I., 2001, *AJ*, 121, 1799
 Péroux C., Dessauges-Zavadsky M., D’Odorico S., Kim T.S., McMahon R., 2003, *MNRAS*, 345, 480
 Péroux C., McMahon R.G., Storrie-Lombardi L.J., Irwin M.J., 2003, *MNRAS*, 346, 1103
 Péroux C., Dessauges-Zavadsky M., D’Odorico S., Sun Kim T., McMahon R.G. *MNRAS*, 363, 479

- Péroux C., Kulkarni V.P., Meiring J., Ferlet R., Khare P., Lauroesch J.T., Vladilo G., York D.G., 2006, *A&A*, 450, 53
- Péroux C., Meiring J., Kulkarni V.P., Ferlet R., Khare P., Lauroesch J.T., Vladilo G., York D.G., 2006, *MNRAS*, 372, 369
- Petitjean P., Webb J.K., Rauch M., Carswell R.F., Lanzetta K., 1993, *MNRAS*, 262, 499
- Pettini M., Ellison S.L., Steidel C.C., Shapley A.E., Bowen, D.V., 2000, *ApJ*, 532, 65
- Pei Y., Fall S.M., Hauser M.G., 1995, *ApJ*, 522, 604
- Prochaska J.X., Wolfe A.M., 1999, *ApJS*, 121, 369
- Prochaska J.X., Wolfe A.M., 2002, *ApJ*, 566, 68
- Prochaska J.X., Howk J.C., O'Meara J.M., Tytler D., Wolfe A.M., Kirkman D., Lubin D., Suzuki N., 2002, *ApJ*, 571, 693
- Prochaska J.X., O'Meara J.M., Herbert-Fort S., Burles S., Prochter G.E., Bernstein R.A., 2006, *ApJL*, in press (astro/0606573)
- Rao S.M., Turnshek D.A., Nestor D.B., 2006, *ApJ*, 636, 610
- Reddy B.E., Lambert D.L., Prieto C.A., 2006, *MNRAS*, 367, 1329
- Richards G.T., Fan X., Schneider D.P., Vanden Berk D.E., Strauss M.A., York D.G., Anderson J.E., Anderson S.F., 2001, *AJ*, 121, 2308
- Rocha-Pinto H.J., Scalo J., Maciel W. J., Flynn C., 2000, *A&A*, 358, 869
- Samland M., 1998, *ApJ*, 496, 155
- Savaglio, S. et al. 2005, *ApJ*, 635, 260
- Schaye J., 2006, *ApJ*, 643, 59
- Tremonti C. A. et al. 2004, *ApJ*, 613, 898
- Timmes, F. X., Woosley S.E., Weaver T.A., 1995, *ApJS*, 96, 617
- Vidal-Madjar A., Laurent C., Bonnet R. M., York D. G., 1977, *ApJ*, 211, 91
- Welty D.E., Hobbs L.M., York D.G., 1991, *ApJS*, 75, 425
- Welty D.E., Frish P.C., Sonneborn G., York D.G., 1999, *ApJ*, 512, 636
- Welty D.E., Lauroesch J.T., Blades C., Hobbs L.M., York D.G., 2001, *ApJ*, 554, 75
- York D.G., Khare P., Vanden Berk D., Kulkarni V.P., Crotts A.P.S., Lauroesch J.T., Richards G.T., et al., 2006, *MNRAS*, 367, 945

This paper has been typeset from a \LaTeX file prepared by the author.

7 APPENDIX

7.1 $N_{\text{H I}}$ Determinations

The systems studied in this work all have known $N_{\text{H I}}$ from HST spectra. For completeness, we provide plots of the Voigt profiles of the Lyman- α transition using the best fit values of the column density from Rao, Turnshek, & Nestor (2006). Due to the low resolution and S/N of these UV spectra, only one component was used in the fits. We show in the following figures the Voigt profiles corresponding to the column densities given by Rao, Turnshek, & Nestor (2006) and convolved with a Gaussian instrumental spread

function based on a two pixel resolution element, superimposed on the archival data from HST cycle 6 program 6577, cycle 9 program 8569, and cycle 11 program 9382. We note that the normalization, i.e., the continuum fit that we define may differ from that adopted by Rao, Turnshek, & Nestor (2006). For Q2051+1950, we have revised the fit of Rao, Turnshek, & Nestor (2006) to $\log N_{\text{H I}} = 20.00 \pm 0.15$. For all other cases, we find their values completely in agreement. For our continuum fits, a polynomial typically of order 5 or less or a cubic spline was used, and the absorption line itself was excluded from the fitting region. Also over-plotted are profiles with H I column densities smaller and larger by 0.15 dex than the best fit values. A bar located below the continuum level in the absorption feature denotes the range of absorption seen in the Mg II profiles in velocity space. For Q0005+0524, a shift of $\sim 200 \text{ km s}^{-1}$ was applied to align the profile due to apparent inaccuracies in the wavelength calibration of the FOS spectrum. See also Miller, Knezek & Bregman (1999) for more on the FOS pipeline wavelength calibration inaccuracies.

Higher resolution UV spectra covering higher Lyman series transitions (Lyman- β , Lyman- γ , etc) would help to resolve the effects of the wide spread of the Mg II components, and discern abundance differences between components which is not possible with the current lower resolution UV spectra.

7.2 Individual Fit Parameters

Here we give the parameters for the fits for each individual system. Radial velocities and effective Doppler parameters of the components are in units of km s^{-1} , while the column densities are in cm^{-2} . The errors for each component are 1σ formal errors from FITS6P.

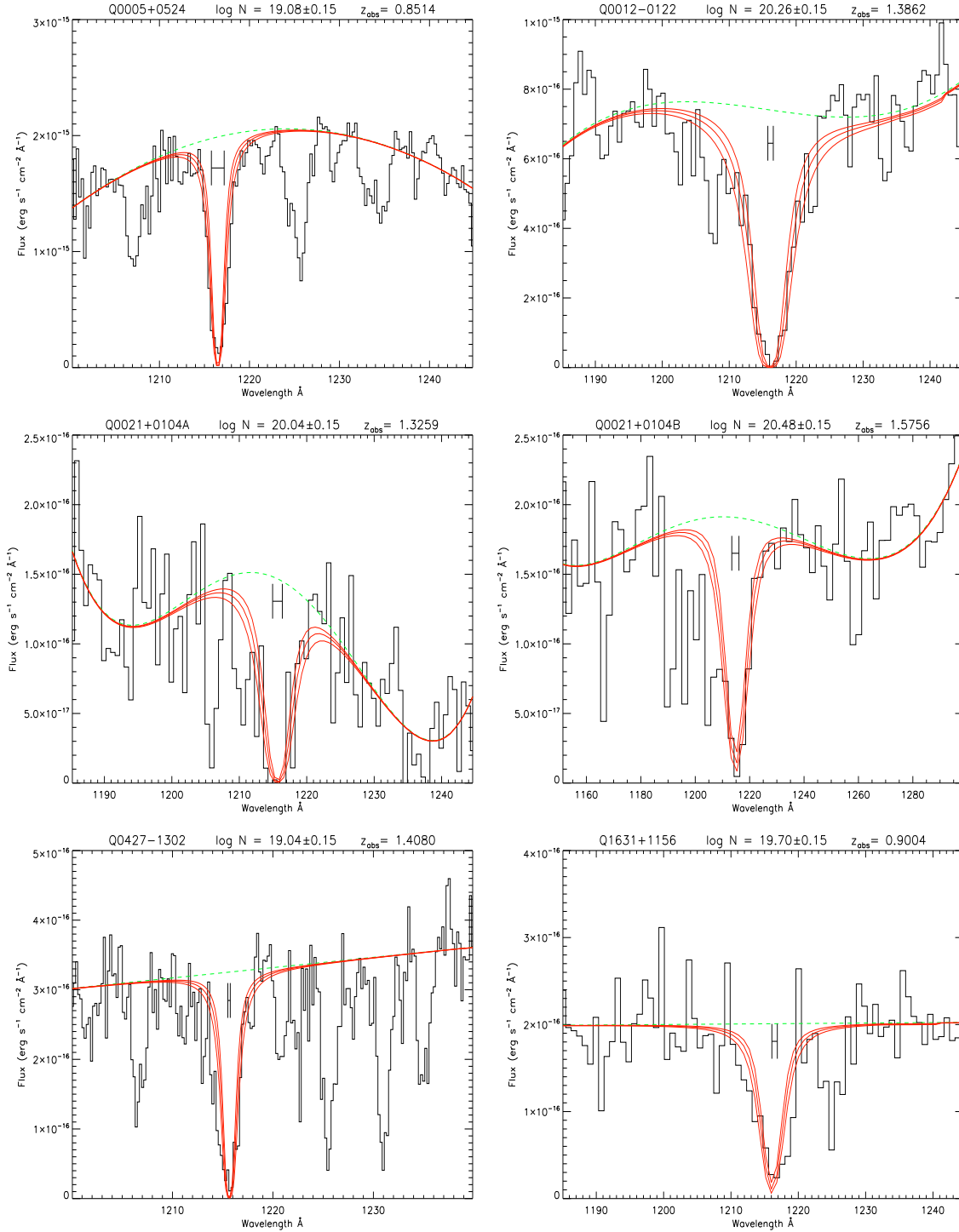
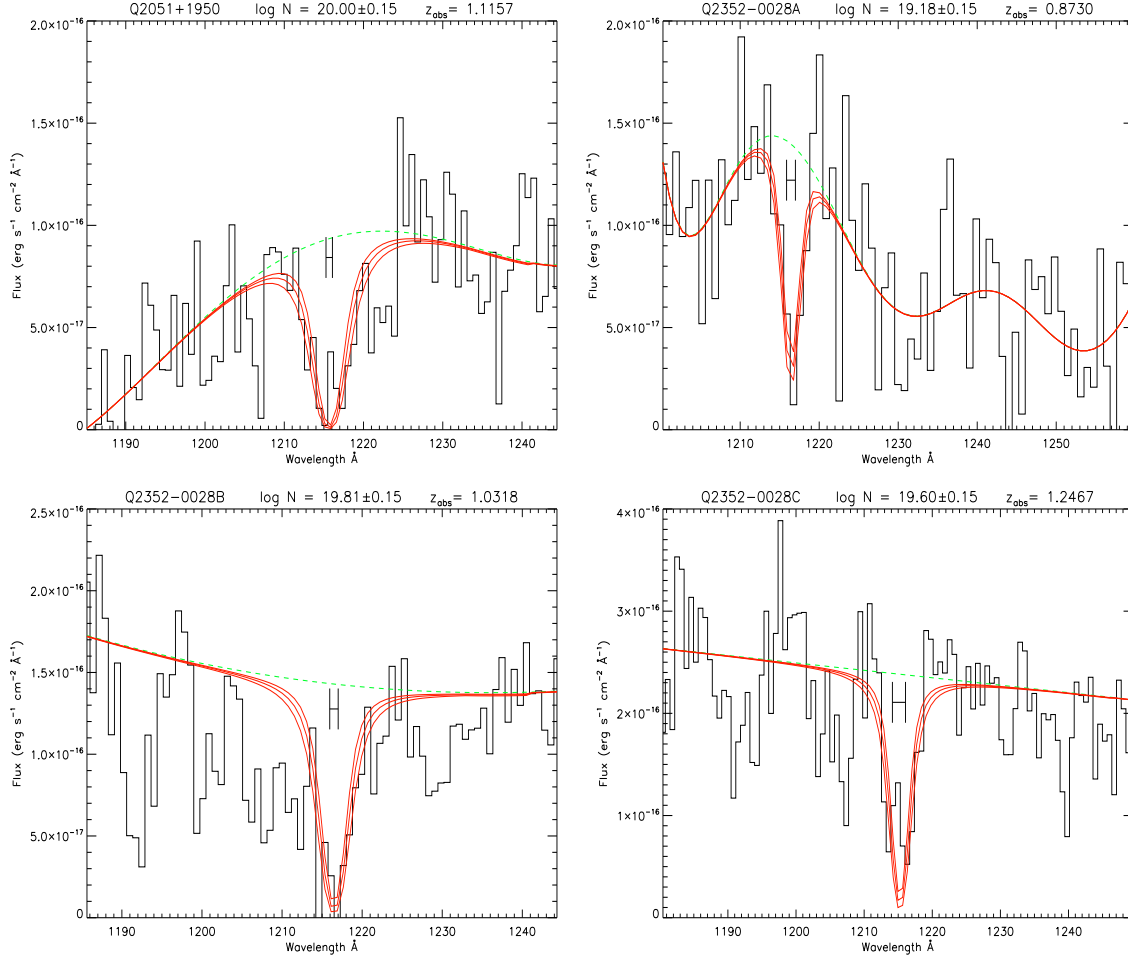


Figure 12. UV spectra of the systems in this sample. The dashed green line indicates the best fit level of the continuum. Superimposed on the data are theoretical Voigt profiles that have been convolved with a gaussian instrumental spread function. The middle profile is the best fit value from Rao, Turnshek, & Nestor (2006), and the upper and lower column densities have been modified by ± 0.15 dex from the best fit value. The bar located below the continuum level in the absorption feature denotes the range of absorption seen in the Mg II profiles in velocity space.

**Figure 13.** Same as Figure 12**Table 5.** Column densities for Q0005+0524, $z_{abs}=0.8514$, $N_{H\ I}=19.08$

v	b_{eff}	Mg I	MgII	Al III	Fe II
-26	8.6	(4.24±0.27)E11	>3.09E13	(2.71±0.53)E12	(1.63±0.04)E13
-11	6.2	(5.55±0.32)E11	>4.18E13	(4.30±0.68)E12	(2.87±0.07)E13
7	5.6	(4.26±0.26)E11	>7.69E13	(1.67±0.43)E12	(1.02±0.03)E13
35	10.3	(9.78±2.09)E10	(3.01±0.21)E12	-	-
145	4.7	-	>8.09E12	(6.10±3.43)E11	(2.36±0.21)E12
182	6.9	-	>4.72E13	(3.44±0.55)E12	(4.01±0.24)E12
301	9.0	-	(9.11±1.39)E11	-	-
412	5.5	-	(1.34±1.55)E12	-	-

Table 6. Column densities for Q0012-0122, $z_{abs}=1.3862$, $N_{H\ I}=20.26$

v	b_{eff}	Mg I	Mg II	Al II	Al III	Si II	Fe II
-61	5.3	-	>1.10E13	(1.16±0.14)E12	-	(4.08±2.27)E13	(1.66±0.18)E13
-43	14.3	(4.40±0.32)E11	>6.38E13	>8.02E12	(2.23±0.15)E12	(1.65±0.41)E13	(1.48±0.05)E14
-2	5.2	(9.32±1.97)E10	>3.23E13	>1.50E12	(3.79±0.16)E12	(4.05±1.44)E13	(4.75±0.56)E12
57	13.7	-	>8.20E12	>8.57E11	(1.32±0.13)E12	(1.39±0.48)E13	(3.39±0.63)E12
97	10.2	-	(2.63±0.11)E12	(2.03±0.57)E11	-	-	-
127	12.7	-	(5.12±0.15)E12	(2.96±0.63)E11	(4.49±1.19)E11	-	(1.15±0.56)E12

Table 7. Column densities for Q0021+0104, $z_{abs}=1.3259$, $N_{H\ I}=20.04$

v	b_{eff}	Mg I	Mg II	Al II	Si II	Fe II
-231	4.1	-	(2.00±0.21)E12	-	-	(2.53±0.90)E12
-166	9.0	-	>1.06E13	>1.28E12	>1.07E13	(9.54±1.23)E12
-127	13.0	-	>6.91E12	>2.04E12	-	(3.78±1.16)E12
-101	8.4	-	>1.27E14	>5.96E12	>8.16E13	(3.42±0.25)E13
-65	9.5	-	>2.31E13	>4.73E12	>3.54E13	(1.95±0.18)E13
-35	13.8	(7.79±0.88)E11	>9.89E13	>1.81E13	>2.64E14	(1.06±0.06)E14
-8	9.0	(6.60±0.83)E11	>1.32E14	>3.56E12	>8.19E13	(7.57±0.54)E13
25	5.7	-	>4.01E13	>9.52E11	>2.84E13	(1.30±0.18)E13
39	6.8	-	>1.04E13	>3.42E12	>6.79E13	(4.02±0.51)E13
55	10.1	-	>1.73E14	>4.44E12	>9.53E13	(9.17±0.66)E13
95	7.2	-	>7.12E13	>2.99E12	>6.42E13	(5.51±0.43)E13
118	14.1	-	>1.82E13	>2.57E12	>4.97E13	(2.21±0.19)E13
145	9.4	-	>6.21E12	-	>6.84E12	(1.29±0.14)E13

Table 8. Column densities for Q0021+0104, $z_{abs}=1.5756$, $N_{H\ I}=20.48$

v	b_{eff}	Mg I	Mg II	Al III	Si II	Fe II
-339	13.6	-	(5.37±0.27)E12	-	(1.05±0.22)E13	(2.16±0.42)E12
-305	8.6	(8.89±3.67)E10	(5.44±0.32)E12	-	(1.22±0.21)E13	(2.79±0.39)E12
-264	6.6	-	(6.87±1.27)E11	-	-	-
-197	5.5	-	(4.00±0.30)E12	-	(5.84±1.64)E12	(2.52±0.37)E12
-145	12.1	-	(3.89±0.28)E12	-	(4.01±0.43)E13	(2.69±0.48)E12
-133	4.3	(8.99±3.54)E10	(4.51±0.77)E12	-	(3.09±2.53)E12	(4.51±0.59)E12
-113	9.2	(4.16±0.47)E11	>6.39E13	-	(1.24±0.20)E14	(2.40±0.14)E13
-87	10.7	(2.79±0.45)E11	>3.11E13	-	(5.65±0.66)E13	(1.53±0.10)E13
-63	10.1	(2.98±0.92)E11	>6.78E13	(1.82±0.32)E12	(8.27±2.27)E13	(6.77±1.05)E13
-56	11.4	(2.17±1.02)E11	>1.47E13	-	(3.05±2.48)E13	(3.49±1.65)E13
-37	13.3	(2.04±0.54)E11	>2.32E13	-	(8.57±0.98)E13	(1.17±0.08)E14
-5	9.7	(2.95±0.44)E11	(6.90±0.39)E12	-	(1.79±0.25)E13	(1.19±0.07)E13
37	9.1	(3.48±0.47)E11	>2.29E13	-	(4.39±0.55)E13	(7.04±0.69)E12
54	10.6	(1.65±0.45)E11	>3.79E13	-	(5.56±0.70)E13	(2.72±0.17)E13
81	11.3	(6.96±0.59)E11	>3.16E13	-	(8.74±1.06)E13	(3.96±0.23)E13
106	11.8	(5.93±0.96)E11	>1.20E13	-	(3.57±1.02)E13	(5.25±2.29)E12
115	12.6	(3.05±0.89)E11	>2.85E13	-	(5.33±0.87)E13	(3.89±0.27)E13
152	9.2	-	(5.46±0.31)E12	-	(1.18±0.21)E13	(2.40±0.38)E12
179	6.4	-	(7.33±1.29)E11	-	-	-
272	4.4	-	(9.17±1.35)E11	-	-	-

Table 9. Column densities for Q0427-1302, $z_{abs}=1.4080$, $N_{H\ I}=19.04$

v	b_{eff}	Mg II	Al II	Si II	Fe II
1	6.9	(5.27±0.31)E13	(1.13±0.07)E12	(3.29±0.21)E13	(2.27±0.07)E13
-50	8.3	(4.38±0.65)E11	-	(3.35±0.87)E12	-
-24	13.2	(1.21±0.09)E12	(4.37±0.61)E11	(3.13±1.02)E12	-

Table 10. Column densities for Q1631+1156, $z_{abs}=0.9004$, $N_{H\ I}=19.70$

v	b_{eff}	Mg I	Mg II	Ca II	Fe II
-67	11.1	-	>1.65E13	-	(1.18±0.06)E13
-35	8.0	(4.39±1.39)E11	>2.69E13	(4.67±1.19)E11	(3.20±0.20)E13
-20	8.5	(1.80±0.30)E12	>2.48E13	(4.27±1.19)E11	(6.24±0.43)E13
6	7.6	-	>7.98E13	(4.70±1.16)E11	(2.13±0.13)E13
56	8.0	-	(3.29±0.29)E12	-	(1.89±0.33)E12
88	10.9	-	(2.29±0.24)E12	-	-

Table 11. Column densities for Q2051+1950, $z_{abs}=1.1157$, $N_{H\ I}=20.00$

v	b_{eff}	Mg I	Mg II	Al II	Al III	Si II
-19	8.1	-	(2.95±0.17)E12	-	-	-
1	10.6	(3.25±0.35)E11	>2.82E13	>9.81E12	(2.64±0.44)E12	-
25	9.6	(7.17±0.44)E11	>8.11E13	>9.09E12	(3.12±0.47)E12	-
51	11.1	(9.24±0.60)E11	>7.42E13	>9.87E12	(4.18±0.65)E12	-
66	8.0	(1.79±0.11)E12	>5.94E13	>8.01E12	(1.03±0.14)E13	(1.01±0.18)E15
88	8.2	(4.00±0.37)E11	>8.17E13	>3.31E12	(5.86±0.74)E12	-
105	7.4	(2.46±0.37)E11	>2.29E13	>3.62E12	(3.48±0.63)E12	-
144	11.9	-	(2.17±0.13)E12	-	(8.78±3.70)E11	-
119	9.8	-	>6.08E13	>6.04E12	(3.34±0.55)E12	(3.94±1.36)E14
v	b_{eff}	Ca II	Mn II	Cr II	Fe II	Zn II
-19	8.1	-	-	-	(2.68±0.71)E12	-
1	10.6	-	(9.91±1.61)E11	-	(8.77±0.40)E13	(7.90±0.92)E11
5	9.6	(7.05±1.29)E11	(2.27±0.18)E12	(2.46±1.15)E12	(1.59±0.09)E14	(1.34±0.09)E12
51	11.1	(1.21±0.17)E12	(2.35±0.21)E12	-	(1.54±0.10)E14	(1.12±0.11)E12
66	8.0	(8.85±1.51)E11	(4.88±0.27)E12	(5.37±1.30)E12	(2.81±0.34)E14	(2.59±0.12)E12
8	8.2	(4.02±1.14)E11	(2.54±0.19)E12	-	(1.85±0.15)E14	(8.77±0.87)E11
105	7.4	(3.49±1.18)E11	(1.55±0.19)E12	-	(1.06±0.09)E14	(3.84±0.90)E11
144	11.9	-	(5.47±1.55)E11	-	(5.22±0.77)E12	-
119	9.8	-	(9.87±1.77)E11	-	(5.83±0.32)E13	(8.01±1.00)E11

Table 12. Column densities for Q2352-0028, $z_{abs}=0.8739$, $N_{H\ I}=19.18$

v	b_{eff}	Mg I	Mg II	Fe II
-146	9.8	-	(1.32±0.15)E12	(5.18±3.11)E11
-122	11.8	-	(4.03±0.23)E12	(1.80±0.35)E12
-94	11.8	-	(1.62±0.16)E12	(1.10±0.34)E12
-46	9.2	(1.91±0.58)E11	>1.41E13	(2.97±0.32)E12
-15	9.0	(2.69±0.67)E11	>2.90E13	(8.25±0.41)E12
0	7.5	(1.33±0.60)E11	>7.27E13	(6.27±0.38)E12
26	6.4	-	>6.27E12	(2.30±0.39)E12
34	7.7	-	>3.92E13	(1.62±0.41)E12
58	5.6	(1.16±0.51)E11	>1.57E13	(4.03±0.30)E12
79	7.4	-	>3.64E12	(1.30±0.29)E12

Table 13. Column densities for Q2352-0028, $z_{abs}=1.0318$, $N_{H\ I}=19.81$

v	b_{eff}	Mg I	Mg II	Al III	Si II	Cr II	Fe II
-111	6.5	-	(1.23±0.15)E12	-	(1.36±0.52)E14	-	(2.26±0.44)E12
-77	11.1	(8.43±0.54)E11	>2.54E14	(1.66±0.47)E12	(2.83±0.65)E14	-	(6.93±0.23)E13
-53	9.4	(5.54±0.78)E11	>1.15E13	-	-	-	(7.02±0.55)E13
-46	8.0	-	>2.83E13	(2.67±0.76)E12	(3.57±1.05)E14	-	(1.07±0.08)E14
-28	7.6	(3.89±0.42)E11	>9.56E13	(3.01±0.49)E12	(2.49±0.60)E14	-	(4.41±0.20)E13
0	8.8	(1.35±0.36)E11	>3.10E13	-	(2.04±0.61)E14	-	(4.99±0.21)E13
18	10.2	(3.08±0.41)E11	>1.31E14	(3.83±0.53)E12	(4.52±0.70)E14	(2.12±0.77)E12	(1.20±0.04)E14
48	6.4	(1.76±0.36)E11	>8.44E13	(2.04±0.44)E12	-	-	(4.24±0.21)E13
66	8.9	(8.84±0.59)E11	>3.00E13	(6.25±0.62)E12	(5.99±0.72)E14	(4.07±0.77)E12	(1.45±0.06)E14
88	8.4	(6.30±0.48)E11	>1.77E14	(6.11±0.60)E12	(4.81±0.67)E14	(2.88±0.72)E12	(1.51±0.06)E14
111	4.0	(9.74±2.96)E10	>1.92E13	-	-	-	(4.71±0.47)E12

Table 14. Column densities for Q2352–0028, $z_{abs}=1.2467$, $N_{H\ I}=19.60$

v	b_{eff}	Mg I	Mg II	Al III	Fe II
–210	9.5	-	>5.33E12	-	(3.37±0.74)E12
–184	10.9	-	>1.98E12	-	-
–152	7.9	(1.49±0.37)E11	>3.60E13	-	(5.71±0.77)E12
–109	12.7	-	>4.54E12	-	-
–87	8.9	-	>6.93E12	(1.41±0.25)E12	(1.79±0.78)E12
–66	9.3	(2.73±0.43)E11	>2.03E14	(7.92±0.53)E12	(4.63±0.23)E13
–31	8.9	-	>1.44E14	(4.27±0.34)E12	(8.28±0.85)E12
6	7.8	(2.88±0.44)E11	>2.15E14	(3.95±0.34)E12	(1.12±0.10)E13
21	5.7	(5.34±0.56)E11	>1.80E14	(1.69±0.25)E12	(2.03±0.15)E13
50	4.0	(2.40±0.41)E11	>5.91E14	(5.28±1.75)E11	(8.61±0.96)E12
77	6.6	-	>1.64E12	-	-
108	11.6	(1.84±0.41)E11	>1.60E13	(1.99±0.27)E12	(5.54±0.82)E12
135	4.5	-	>2.78E12	-	(2.79±0.67)E12
163	10.5	(4.83±0.48)E11	>3.40E14	(2.53±0.28)E12	(4.93±0.22)E13
202	7.9	-	>2.19E12	-	-